Shock-to-detonation transition of nitromethane: Time-resolved emission spectroscopy measurements

Viviane Bouyer, Isabelle Ranc-Darbord, Philippe Hervé, Gérard Baudin, Christian Le Gallic, François Clément, Guy Chavent

Shock-to-detonation transition of nitromethane: Time-resolved emission spectroscopy measurements

Viviane Bouyer [a,1], Isabelle Darbord [a,*], Philippe Hervé [a], Gérard Baudin [b], Christian Le Gallic [b], François Clément [c], Guy Chavent [c]

[a] *Laboratoire d'énergétique et d'économie d'énergie, Université Paris X, 1 Chemin Desvallières, F-92410 Ville d'Avray, France*
[b] *Centre d'études de Gramat, DGA/DCE/CEG, F-46500 Gramat, France*
[c] *INRIA-Rocquencourt, BP105, F-78153 Le Chesnay Cedex, France*

Abstract

The objective of this work is to improve the knowledge of the shock-to-detonation transition of nitromethane. The study is based on a spectral analysis in the range 0.3–0.85 µm, with a 28-nm resolution, during experi-ments of plane shock impacts on explosive targets at 8.6 GPa. The time-resolved radiant spectra show that the detonation front, the reaction products produced during the superdetonation, and the detonation products are semitransparent. The temperature and absorption coefficient profiles are determined from the measured spectra by a mathematical inversion method based on the equation of radiative transfer with Rayleigh scattering regime. Shocked nitromethane reaches at least 2500 K, showing the existence of local chemical reactions after shock entrance. Levels of temperature of superdetonation and steady-state detonation are also determined.

Keywords: Nitromethane; Shock-to-detonation transition; Emission spectroscopy; Temperature profile; Absorption coefficient models; Inverse problems; Equation of radiative transfer

1. Introduction

This work deals with the study of the shock initiation of a liquid high explosive, nitromethane (NM). Many experimental investigations as well as theoretical researches have been performed on NM for about 40 years but the detonation mechanisms are not still completely explained. Their understanding rests mainly on pressure and velocity measurements. However, to improve knowledge of the initiation and detonation of high explosives, temperature is an essential factor. It is of great interest for the understanding of the involved chemical kinetics, for the accuracy of hydrodynamic codes related to condensed explosives, and for the characterization of the thermal effects of high explosives.

For many years a nonintrusive technique, optical pyrometry, has been used to get the temperature during the shock-to-detonation transition (SDT) of NM and also during the detonation of very nonideal high explosives [1,2]: it has a response time of only a few nanoseconds, compatible with the swiftness of

* Corresponding author. Fax: +33 1 4709 4568.
E-mail address: isabelle.darbord@u-paris10.fr (I. Darbord).
[1] Now at CEA Le Ripault, BP16, F-37260 Monts, France.

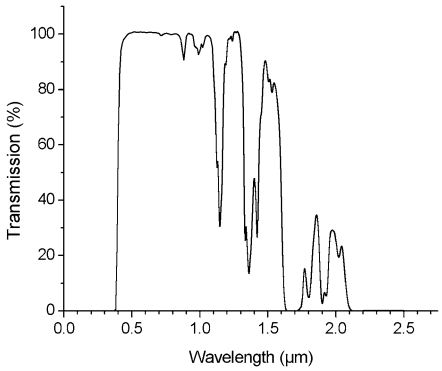

Fig. 1. Transmission spectrum of NM for a thickness of 25 mm measured by a FT-IR Fourier spectrometer.

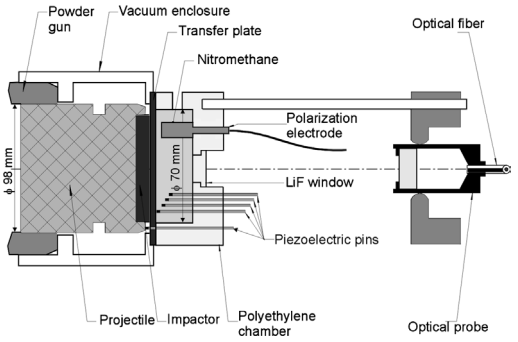

Fig. 2. Detonation target.

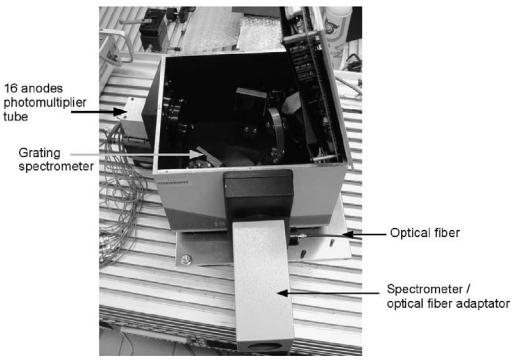

Fig. 3. Emission spectroscopy device.

the phenomena. However, the temperature determination, based on thermal radiation emitted by the explosive, requires knowing the emissivity of the gaseous or solid species involved during the SDT. This parameter is not measurable under such conditions of pressure (several GPa) and temperature (several thousands of K). These thermodynamic states peculiar to detonation are not easily reachable and most of the techniques used to determine the emissivity in static states [3,4] are unable to get sufficient temporal resolution. Moreover, the modeling of emission spectra from databases is restricted to lower pressures and temperatures corresponding to combustion [5–7]. That is why temperature determination by pyrometry is based on an assumption on the monochromatic emissivity ε_λ. The simplest solutions consist of black ($\varepsilon_\lambda = 1$) or gray ($\varepsilon_{\lambda 1} = \varepsilon_{\lambda 2}$) body hypotheses [8,9]: if the wavelengths of the pyrometer are remote, the determination of the temperature is inaccurate. The development of multichromatic pyrometers [10], such as the six-wavelength pyrometer of the CEG [11], leads to different solutions: the emissivity is stated as a polynomial of the wavelength λ [12,13]. In the case of NM, the reaction and the detonation products are probably semi-transparent and the previous assumptions may then be unsuitable.

Therefore, to get still more information on the optical properties of the initiation and detonation products, a time-resolved emission spectroscopy technique has been developed and used to analyze plane shock impacts on NM targets [14]. These measurements give the radiation emitted by the explosive as spectral radiance. It is possible to determine the temperature profiles (spatial and temporal distributions) from the radiance values. These two data are linked by the equation of radiative transfer. In this paper, we determine the temperature using a method based on the mathematical inversion of the equation of radiative transfer of a semitransparent medium.

2. Experimental configuration

NM is a liquid explosive that has the property of semitransparency at ambient pressure and temperature. We measured its transmission spectrum for a thickness of 25 mm (Fig. 1): NM is transparent between 0.4 and 0.85 µm.

The detonation experiments consist of plane shock impacts on explosive targets at 8.6 GPa, under conditions of one-dimensional strain. These experiments have been performed previously for pyrometry measurements [15]. A single-stage powder gun propels the projectile at the target at a velocity of 1940 m/s to initiate the detonation. NM is confined in a polyethylene chamber of depth 25 mm, closed on one side by a copper transfer plate and on the other side by a lithium fluoride window (LiF) (Fig. 2). Several measurement techniques are used: a polarization electrode records the time of shock entrance and the time of formation of the superdetonation and the detonation, piezo-electric pins signals lead to the measurement of the shock and detonation velocities.

An optical probe using achromatic doublets collects the radiation emitted during the detonation and transmits it to the emission spectroscopy device (Fig. 3) with an optical fiber. The optical probe has been designed to collect thermal radiation be-

Table 1
Characteristics of plate impact shots

	Shot No.			
	76	1020	1045	2019
V (m/s)	1926	1937	1936	1946
p (GPa)	8.57	8.64	8.64	8.7
t_1 (μs)	1.7	1.65	1.38	1.6
t_2 (μs)	2.36	2.15	1.84	2.15

tween 0.3 and 1.6 μm and the focus area has a 2-mm diameter. The optical fiber is a 1-mm core silica fiber transmitting in the same spectral range. A JOBIN YVON TRIAX 180 grating spectrometer disperses the light beam. The grating, blazed at 0.5 μm, has a groove density of 150 g/mm. The dispersion is 32.8 nm/mm at the wavelength 565 nm. A HAMAMATSU R5900U-01-L16 multianode photomultiplier tube (PMT) is used as a 16-detectors array to detect the signal in the spectral range 0.3–0.85 μm with a response time of 0.6 ns. The detectors are 0.8 mm large and 16 mm high and separated by a 0.2-mm space. Four TEKTRONIX TDS684 digitizers are used for data acquisition. During impact experiments, time sampling is 1 GHz. The time and spectral resolutions obtained are respectively 1 ns and 32 nm, each channel of the PMT detecting light flux on a 26-nm-wide spectral range.

The spectroscopy system has to be calibrated to get a conversion between the radiance (thermal radiation) and the voltage output (or current for the PMT). Because of the relatively high spectral resolution, the 16 channels of the PMT may be considered as monochromatic. A MIKRON M390 black body source is used to perform the calibration (900–3300 K).

3. Experimental results

We have performed several experiments of plate impacts at ∼8.6 GPa on 25-mm-thick NM targets at ambient pressure. Table 1 shows the characteristics of these shots: V is the projectile velocity, p is pressure, t_1 is the time of formation of the superdetonation, and t_2 is the time of formation of the strong detonation according to the classical model of the shock-to-detonation transition (SDT) proposed by Chaiken [16]. The emission spectroscopy measurements are reproducible in terms of radiance signals versus wavelength.

Here we analyze one of our experiments. Fig. 4 represents the 3D radiance profiles obtained during shot 1020 and a typical temporal profile at a given wavelength. Emission spectroscopy measurements with the piezoelectric pins and electrode signals clearly show the different stages of the SDT as

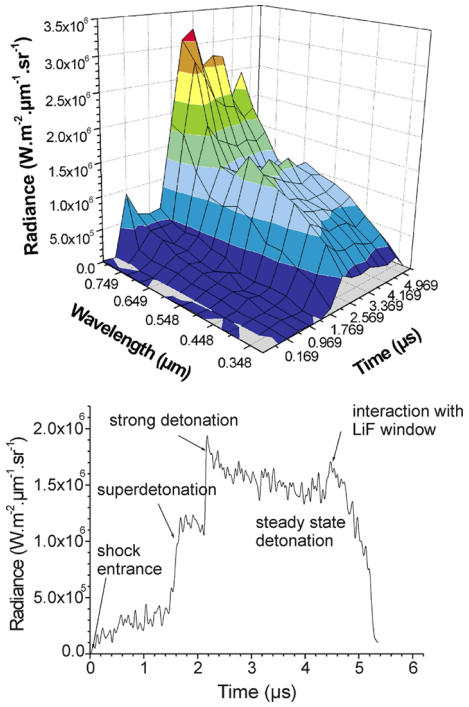

Fig. 4. 3D radiance profiles of shot 1020 and one typical temporal profile.

described by Chaiken. A first jump at 1.65 μs characterizes the formation of a detonation wave propagating in shocked NM resulting of a thermal explosion. This wave is called superdetonation and overtakes the initial shock wave at a second jump at 2.15 μs. A strong detonation is then formed and gradually decays into a steady-state detonation that propagates until the interaction with the LiF window at 4.5 μs.

Radiance temperature (T_{radiance}) profiles (also called brightness temperature profiles) have been calculated with the Planck law, assuming the emissivity ε_λ is 1, i.e., emissivity of a black body:

$$T_{\text{radiance}} = \frac{C_2}{\lambda \ln\left[\frac{C_1 \lambda^{-5}}{L_{\lambda\,\text{mes}}} + 1\right]} \tag{1}$$

with λ for the wavelength, $L_{\lambda\,\text{mes}}$ for the measured radiance, $C_1 = 3.741 \times 10^{-16}$ W m^2, and $C_2 = 1.4388 \times 10^{-2}$ m K are constants of the Planck law.

The true temperature will be at least equal to the maximum radiance temperature.

Because of the noise of the system, minimum temperature corresponding to the measured radiance is about 1500 K. The main result is that the radiance temperature is not constant during the propagation of the superdetonation and the detonation wave (Fig. 5). The reaction products, which consist of gaseous species and solid carbon, are probably semi-

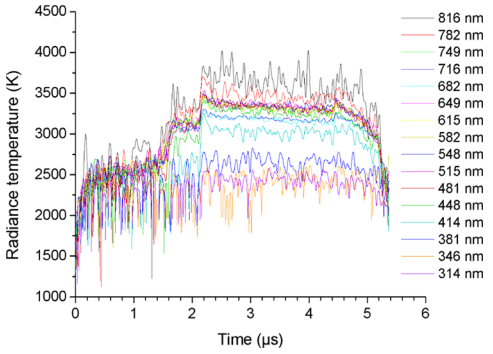

Fig. 5. Radiance temperature profiles for the 16 channels of shot 1020.

Table 2
Minimum temperature of the different stages of the SDT

Stage of the SDT	Temperature (K)
After shock entrance	⩾2500
Before the superdetonation formation	⩾2600
Superdetonation	⩾3200
Detonation	⩾3600

transparent. We obtain the minimum temperature for each step of the SDT that are shown in Table 2.

Experimental uncertainties have been studied in [17]. For low wavelengths (<0.5 µm) and low temperatures (<1500 K—noise limit), the error on radiance can reach 60%. But this error decreases when the temperature increases and is lower than 10% for temperatures higher than 1800 K and for all wavelengths. On the contrary, the error on radiance temperature is negligible (lower than 0.6% in all cases).

Changes in radiance depending on wavelength have been studied for various typical stages of the SDT (Fig. 6). From the formation of the superdetonation, a hollow appears between 0.65 and 0.75 µm. It remains until the end of the propagation of the detonation wave. This hollow characterizes semitransparent optical properties of the gaseous species involved.

4. Discussion

We compared our measurements to those obtained by the pyrometry technique, in particular results from Leal-Crouzet et al. [1] and Urtiew [18] (Fig. 7). Urtiew emission results put in evidence the wavelength dependence on radiance temperature. It is thus not likely that the detonation wave behaves as a black body as proposed by Leal-Crouzet and other authors [19,20], who obtained constant radiant temperature. Their results can be explained by the larger spectral resolution they are using (two or three times larger than ours); the wavelength dependence on the

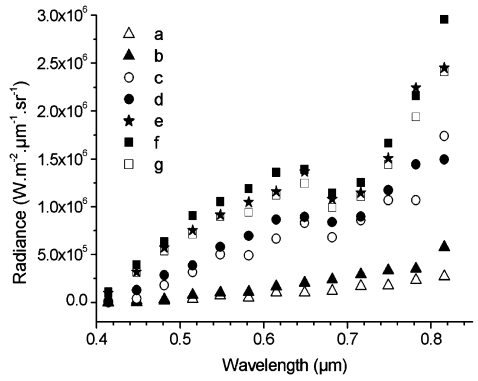

Fig. 6. Radiance spectra at different times for shot 1020: (a) after shock entrance (0.3 µs), (b) before the superdetonation formation (1.2 µs), (c) superdetonation formation (1.65 µs), (d) 1.9 µs, (e) catch-up of the shock wave (2.15 µs), (f) strong detonation (2.45 µs), (g) overdriven steady state detonation (3.8 to 4.4 µs). Radiance values were averaged around the given time value.

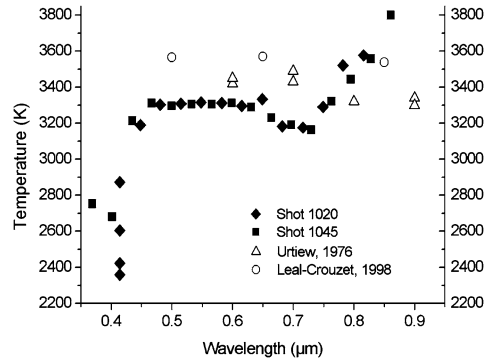

Fig. 7. Radiance temperature of detonation wave of nitromethane versus wavelength compared to other works.

emissivity is then integrated. The choice of the pyrometer wavelengths can thus affect the estimation of the optical characteristic of the studied medium [21].

Then we tried to find out the optical properties of shocked NM and of the reaction products behind the superdetonation wave and behind the detonation wave.

The evolution of the signal emitted after the shock entrance leads us to conclude that the shock front is transparent. Indeed, if the shock front were opaque, the emitted radiance would be constant until the formation of the strong detonation. Moreover, the radiance is about the same as the radiance emitted by the copper impactor at 500 K [17]. This means that shocked NM is transparent and we will consider that its absorption coefficient is the same as that for neat NM. Besides, Yoo et al. [22] pointed out that shocked NM remains transparent in the spectral range 0.35–0.75 µm.

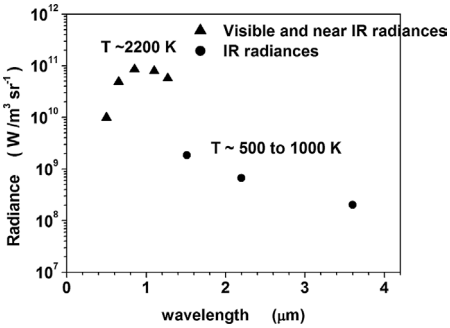

Fig. 8. Radiation emitted during multiple reverberating shocks experiments performed in CEG [25].

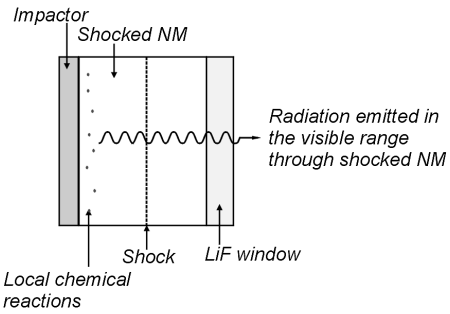

Fig. 9. Radiation emitted during the propagation of the shock wave.

The radiant temperature after shock entrance, prior to the detonation transition, reaches 2500 K. Such a temperature is not in agreement with Chaiken model, which predicts a shock temperature of about 1000 K. It is also clearly greater than those predicted by Lysne and Hardesty [23] (1100–1200 K) or Winey and Gupta [24] (1000 K). Yet a similar high temperature has been also recorded by pyrometry technique in the visible range in the same single sustained shock experiments [15] and in multiple-shock experiments performed at the CEG [25,26]. The reverberating shock tests described in [26] consist in pyrometry measurements (eight wavelengths from visible, 0.5 μm, to IR, 3.6 μm, with 5 ns time resolution) and material velocity measurements using VISAR. In this work, it appears that the temperature profile in the NM layer after the fourth shock wave (13.2 GPa) is not uniform (see Fig. 8). Indeed, for visible and near IR wavelengths of the pyrometer where NM is transparent (same wavelength range as our emission spectroscopy device), shocked NM reaches temperatures greater than 2200 K. On the contrary, measurements in IR range (2.2 and 3.6 μm) lead to radiance temperatures between 500 and 1000 K which is more in agreement with Chaiken model. At these wavelengths, NM is opaque and these low temperatures correspond to shocked NM at the interface with the pyrometry measurement window. Thus, the higher temperatures are necessarily located close to the aluminum transfer plate and can be explained by the presence of local decomposition reactions inside the shocked liquid NM, leading to hot spots. The authors also noticed that the intensity of the laser in the VISAR signals recorded at the transfer plate/NM interface do not decrease, which implies that there is not a bulk decomposition of NM. These results support the presence of these local reactions, created after the passage of shock waves on bubbles and heterogeneities inside NM. These hot spots contribute to increase the radiance measured in the visible range without changing the optical properties of neat NM. The mechanism of emission is shown in Fig. 9.

The chemical composition of the reaction and detonation products has been calculated with the CHEETAH code [27] using two classical equations of state and several data bases. Table 3 shows the major species (with a molar fraction greater than 1%), gas and carbon clusters which form a semitransparent medium [17,21]. The radiation emitted by this medium is given by the complete equation of radiative transfer (ERT),

$$\frac{\mathrm{d}L_\lambda(\vec{i})}{\mathrm{d}x} = K_\lambda L_\lambda^0(T) - \beta_\lambda L_\lambda(\vec{i}) + \frac{\sigma_\lambda}{4\pi}\int_{4\pi} L_\lambda(\vec{i}')\Phi_\lambda(\vec{i}'\to\vec{i})\,\mathrm{d}\Omega(\vec{i}'), \quad (2)$$

with β_λ the extinction coefficient such as $\beta_\lambda = K_\lambda + \sigma_\lambda$; $K_\lambda(\lambda, T)$ and σ_λ are absorption and scattering coefficients; $L_\lambda(\vec{i})$ is the spectral radiance in the direction $\vec{i}$, $\mathrm{d}\Omega(\vec{i})$ is the solid angle centered in the direction $\vec{i}$, and Φ_λ is the spectral scattering phase function [28]. The scattering phase function represents the probability of the scattering of the radiation coming from the direction $\vec{i}'$ toward direction $\vec{i}$.

Carbon cluster size has been estimated as 50 Å by Winter and Ree [29]. Their particle size parameter x ($x = \pi d/\lambda$, where d is the particle diameter or size of the cluster) is between 0.02 and 0.04 for λ between 0.4 and 0.85 μm. The scattering regime of carbon is therefore Rayleigh scattering. Thus, the ERT is simplified:

$$\frac{\mathrm{d}L_\lambda}{\mathrm{d}x} = K_\lambda L_\lambda^0(T) - K_\lambda L_\lambda(x). \quad (3)$$

In a first stage, we have studied the optical properties of the detonation products during the propagation of the steady-state detonation. According to the Chapman–Jouguet theory, the temperature profile behind the detonation front is constant. Thus, K_λ only depends on λ and during this stage, the measured radiation $L_\lambda(\ell)$ can be written with the equation of

Table 3
Chemical composition (in mol/mol of explosive) of the reaction products from a steady-state detonation of NM calculated with CHEETAH using two classical equations of state (BKW and JCZ3) and several data bases (Lawrence Livermore National Laboratory BKWC, Sandia National Laboratory BKWS and JCZS)

	EOS BKW data base BKWC LLNL			EOS BKW data base BKWC SNL			EOS JCZ3 small data base JCZS SNL		
	Det.	V cste expl.	Super det.	Det.	V cste expl.	Super det.	Det.	V cste expl.	Super det.
P (GPa)	11.4	14.0	25.1	13.2	17.0	31.6	11.7	14.9	27.4
T (K)	3666	3094	3509	3626	2914	3317	3442	2935	3123
H_2O	1.397	1.492	1.499	0.646	0.665	0.608	0.857	0.974	0.827
N_2	0.499	0.500	0.500	0.558	0.449	0.429	0.458	0.460	0.479
CO	0.358	0.134	0.061	0.070	–	–	0.538	0.212	0.119
CO_2	0.120	0.186	0.219	0.558	0.593	0.534	0.254	0.362	0.412
H_2	–	–	–	0.112	–	–	0.230	0.062	0.036
CH_4	0.032	–	–	0.165	0.159	0.081	–	–	–
H_3N	–	–	–	0.092	0.101	0.140	0.083	0.079	0.042
C_2H_6				0.052	0.082	0.108	0.073	0.098	0.152
CH_2O_2	–	–	–	0.075	0.066	0.154	0.041	0.044	0.115
C(s)	0.466	0.674	0.719	0.000	0.000	0.000	0.000	0.182	0.049

Notes. Det.: detonation. V cste expl.: constant volume explosion at 8.6 GPa, 1.842 g/cm^3 (shocked NM). Super det.: detonation wave propagating in compressed NM, i.e., superdetonation wave.

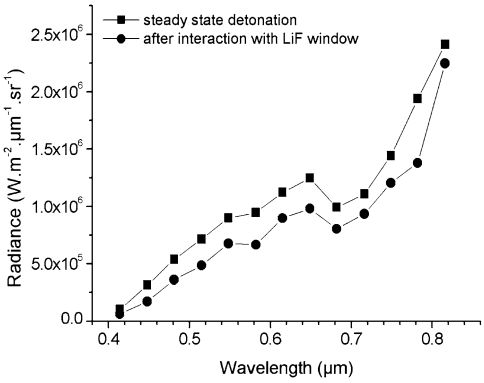

Fig. 10. Comparison of the radiance spectra before and after the interaction with the LiF window.

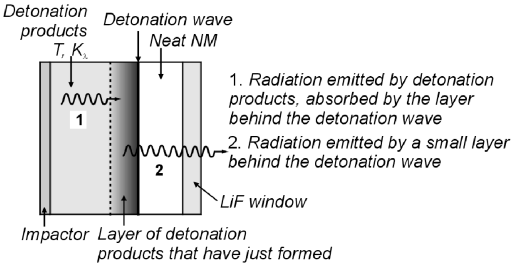

Fig. 11. Radiation emitted during the propagation of the steady-state detonation.

radiative transfer,

$$L_\lambda(\ell) = L_\lambda^0(\mathrm{T})\left[1 - \exp\left(-K_\lambda(x_\mathrm{D} - x_0)\right)\right], \qquad (4)$$

where ℓ is the cell depth, T is the detonation products temperature, K_λ is the absorption coefficient of the detonation products, and x_D and x_0 are the detonation front and impactor/explosive interface positions.

According to Eq. (4), the radiance should increase when the detonation wave moves forward as $(x_\mathrm{D} - x_0)$ increases, but we can notice in Fig. 4 that the emitted radiation before the interaction with the LiF window is constant. It could be explained by surface area emissivity of the detonation front. Yet, the radiance temperature values obtained during the detonation propagation show a deviation of about 500 K depending on the wavelength (Fig. 5). This confirms that the detonation products are semitransparent. Moreover, we can see in Fig. 10 that the shape of the radiant spectrum is the same before and after the interaction with the window. That would not be possible in the case of an opaque detonation front.

The constant signal is more likely due to the fact that the radiation comes from a small thickness behind the detonation wave, remaining constant during the propagation (see Fig. 11). The detonation products can be considered optically thick. The emission spectroscopy system measures the radiation emitted by detonation products that have just formed. Indeed, the same shape obtained in Fig. 10 for the radiance curves before and after the interaction with the LiF window means that the same chemical species are emitting.

The reaction products behind the superdetonation wave are also semitransparent. Indeed, Doppler laser interferometry measurements [25] performed at the CEG show that the laser beam at 0.6 µm crosses the reaction products thickness. By focusing on the signal emitted during the propagation of the superdetonation, it seems that for wavelengths higher than 0.6 µm, the signal is constant, whereas under 0.6 µm, it in-

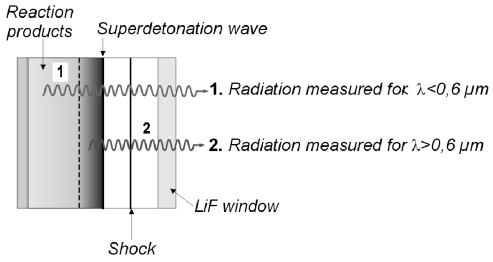

Fig. 12. Radiation emitted during the propagation of the superdetonation wave.

creases. The limit 0.6 µm is not accurate because of the temporal and spectral resolutions of the recording. In order to precise it, it would be necessary to perform measurements with a higher time sampling implying that acquisition is stopped before the end of the propagation. Moreover, to increase spectral resolution, the grating or the detectors have to be changed.

However, we can already analyze the differences between the two spectral regions. Fig. 12 represents this emission mechanism. In the region 0.6–0.85 µm (radiation 2 in figure), reaction products behind the superdetonation behave as detonation products; i.e., the emitted radiation comes from a layer of products behind the superdetonation front. The reaction products are said to be optically thick. In contrast, in the region 0.3–0.6 µm (radiation 1 in figure), reaction products are transparent.

The results obtained on the optical properties of shocked NM and reaction and detonation products lead us to try to find out which species cause the hollow in the radiance spectra. The knowledge of the optical parameters as emissivity or absorption factor is still rather weak. Therefore, only a mathematical inversion of the equation of radiative transfer allows determining both temperature profiles and absorption coefficient.

5. Determination of temperature profiles and absorption coefficient

The inversion consists in determining the temperature profile and the absorption coefficient for each wavelength from the experimental radiance spectra, as functions of time and position. This work is based on the automated determination of physical properties of detonation (temperature, celerity) and absorption coefficient of the medium in the successive stages of the shock to detonation transition by trying to reproduce at best the experimental measurements. The identification is achieved by a least square algorithm, applied to the equation of radiative transfer for a semi-transparent medium in the Rayleigh approximation (Eq. (3)) [21].

In order to dramatically reduce the number of unknowns, we introduce a parameterization of temperature and absorption coefficient. We first take advantage of the fact that the different species encountered at the different stages of the shock to detonation transition always correspond to different values of the temperature. Hence, the absorption coefficient for each wavelength can be seen as a function of the sole temperature. As described in [30,31], the shape of the absorption coefficient is estimated from the analysis of the radiance spectra when the steady state detonation is reached. Then, we notice that the temperature profile presents shocks (reactive or nonreactive) that move at various speeds. This is the typical shape of the solution of a scalar conservative law. So we take the temperature as the solution to a convection–diffusion problem of the form

$$\frac{\partial T}{\partial t} + \frac{\partial f(T)}{\partial x} = g\big(T(x,t)\big), \tag{5}$$

where $f(T)$ is an advection term and $g(T)$ a reaction term.

The parameters to be determined have been chosen according to a sensitivity analysis taking into account the noise level of the experiment. The number of parameters was further reduced with additional information on absorption coefficient and by searching the temperature profile among a limited family that is physically admissible, through specific choices for the advection term f and the reaction term g.

The least-squares approach consists in minimizing the normalized quadratic criterion

$$\tilde{J}(L^{\mathrm{cal}}) = \sum_{k,j}\left(\frac{L_j^{\mathrm{mes},k} - L_j^{\mathrm{cal},k}}{\sigma_j^k}\right)^2 \Bigg/ \sum_{k,j}\left(\frac{L_j^{\mathrm{mes},k}}{\sigma_j^k}\right)^2, \tag{6}$$

where L^{mes} is the measured radiance, L^{cal} is calculated with ERT from the selected temperature and absorption coefficient, and σ stands for the noise and relative errors of measurements. The indices j and k respectively stand for wavelengths and time steps. This definition of the normalized criterion makes it possible to compute the percentage of retrieved radiance profile through $1 - \sqrt{\tilde{J}}$.

The difficulties and the details of the inversion method are described in [17,30,31]. The inversion algorithm has been validated for simple cases of detonation as steady-state detonation and detonation with reaction products relaxation [30,31].

We present here the results of the inversion method applied to the experimental radiance profiles we measured during shot 1020. The computation is divided in

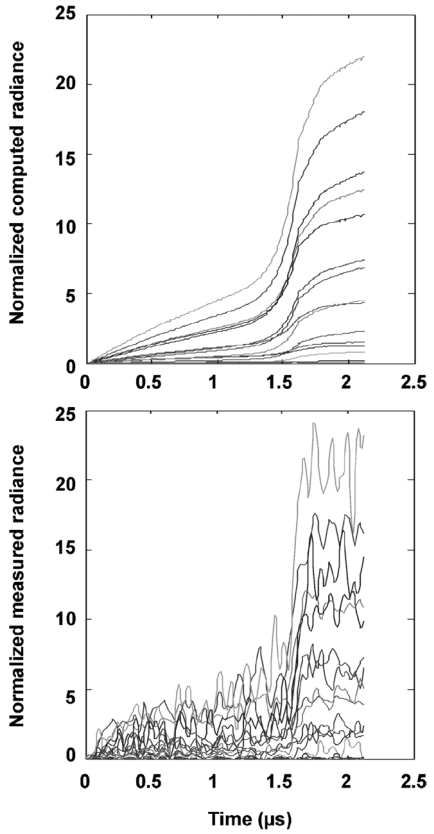

Fig. 13. Comparison of the computed (retrieved) radiance and the measured radiance profiles during SDT.

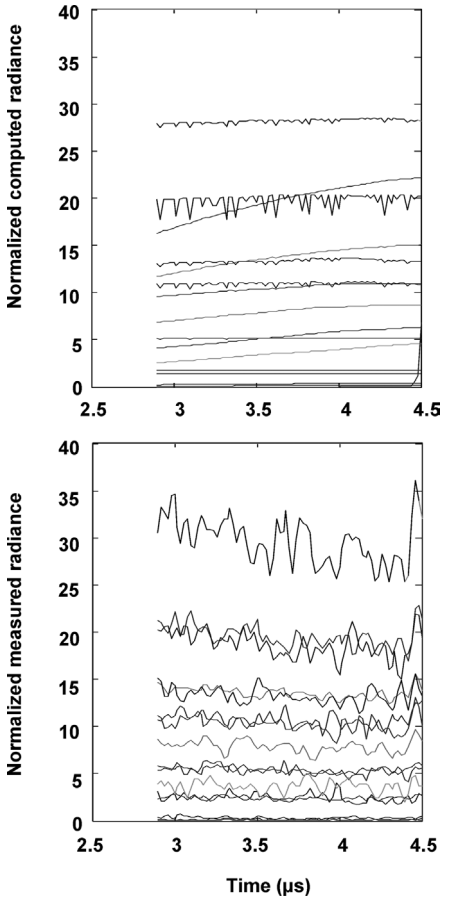

Fig. 14. Comparison of the measured radiance and the computed radiance profiles during the propagation of the detonation.

two steps: the first one consists in retrieving the signal between the shock entrance and the overtaking of the shock wave by the superdetonation wave (identified parameters are the temperature just behind the shock front, the temperature just behind the superdetonation front, and the celerity of the superdetonation front); the second one consists in retrieving the signal during the propagation wave until the interaction with the LiF window (identified parameter is the detonation temperature). The recorded radiance profiles between 2.12 and 2.9 µs correspond to the propagation of the strong detonation with a temperature profile which is difficult to model. This part of the signal was not processed.

5.1. SDT phase between 0 and 2.12 µs

The sensitivity analysis showed a low sensitivity of the measured radiance with respect to the celerity of the superdetonation front. A boundary on celerity has been introduced to limit its value to a physically acceptable range.

Fig. 13 shows computed and measured radiance profiles for several wavelengths; 83% of the radiance profiles are retrieved. The oscillations visible on the measured radiance profiles do not penalize the criterion $\tilde{J}$, which is due to the use of the L^2 norm.

5.2. Detonation–propagation phase between 2.9 and 4.5 µs

In this case, 89% of the radiance profiles are retrieved (Fig. 14). The search for the temperature profile has been reduced to the search for a constant temperature profile. Indeed, difficulties still remain in the inversion of the release of the reaction products part of the profile.

Fig. 15 shows the temperature profiles versus position in the explosive cell for both stages, SDT and detonation propagation. The inversion gives one profile every 10 ns but fewer profiles are drawn on the figure for more clarity. The shock temperature value T_S thus determined is 2810 K, the superdetonation temperature value once the wave is sustained, T_{SD}, is 3166 K, and the detonation temperature T_D is 3253 K.

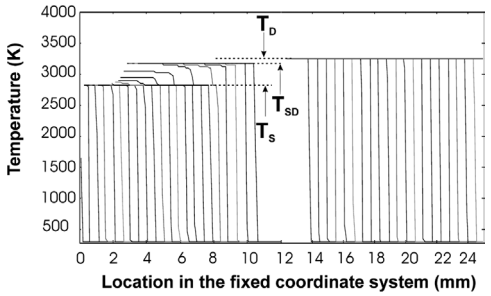

Fig. 15. Temperature profiles versus position obtained by the inversion method.

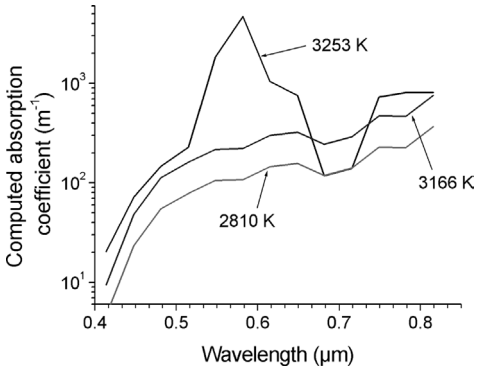

Fig. 16. Computed absorption coefficient at shock (2810 K), superdetonation (3166 K), and detonation (3253 K) temperatures.

At the entrance of the shock, the result shows high temperatures, which confirms the existence of hot spots, due to local chemical reactions, as explained earlier.

Taking into account the noise level of the radiance measurements, the proportion of retrieved radiance profiles is rather high. However, apart from the shock temperature, the superdetonation and the detonation temperature are a bit lower than the minimum temperature given by the brightness temperature we determined from the emission signals (Table 2). The relative error in superdetonation temperature compared to this minimum is 1.1% and the relative error in detonation temperature is 9.6%. The inversion method gives relevant results for the SDT phase but for the detonation–propagation phase, the temperature is rather weak because the calculation was based on the search of a constant temperature profile, whereas it is possible that the steady-state detonation was not already reached.

5.3. *Absorption coefficient profiles*

Fig. 16 shows the computed absorption coefficient during SDT and steady-state detonation (for wavelengths lower than 0.4 μm, NM is opaque).

Table 4
Position and intensity of absorption lines of water vapor [36]

Wavelength (μm)	Intensity (a.u.)
0.698	0.2
0.724	1.08
0.823	0.93
0.906	2.4
0.942	10
0.977	2.1

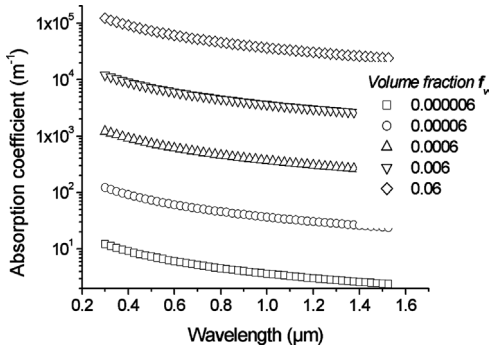

Fig. 17. Absorption coefficient of carbon clusters with varying volume fraction according to Rayleigh scattering.

Among the major species listed in Table 3, only two species in the reaction products emit in the wavelength measurement range: carbon clusters [32] and water vapor (main lines are given in Table 4 at 0.72 and 0.82 μm). We cannot define a more accurate equation of state because the detonation velocities calculated with CHEETAH agree well with experimental data. Therefore concentrations are only indicative.

The calculated volume fraction of carbon varies from 0 up to 9% depending on the equation of state. So, in a first approximation, we choose to represent the Rayleigh scattering regime of the particles by an independent regime [30,33]. The absorption coefficient of particles for different volume fractions f_v is shown on Fig. 17 with a refractive complex index $1.8 - 0.9i$ [32]. Carbon particles produce a continuous background. Comparing these predicted values with the computed absorption coefficient (Fig. 16), we can deduce that the volume fraction of carbon is very small ($<10^{-3}$%). This result is more in agreement with the data base of the Sandia National Laboratory for the gaseous BKW and JCZ3 equations of state.

Regarding the contribution of water vapor, a model is required to represent the absorption coefficient depending on wavelength. The model proposed for the emission of water vapor in the reaction products is simple in view of the lack of knowledge on the emission of gases at the pressure and temperature encountered. It is based on the absorption lines

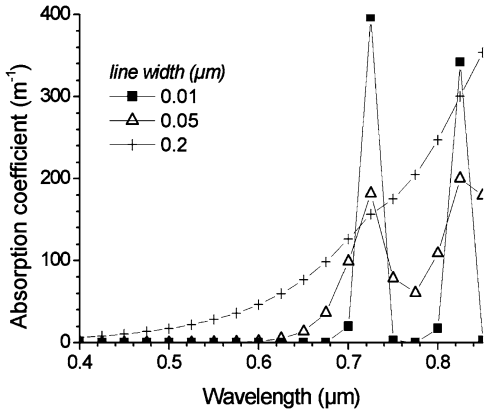

Fig. 18. Absorption coefficient of water vapor calculated with Eq. (4).

of H_2O in the visible range and near-infrared range at ambient pressure and temperature (Table 4) and on a representation of the line width with the exponential wideband model of Edwards [32] that qualitatively considers line broadening with temperature and pressure. Fig. 18 represents the absorption coefficient calculated with the same bandwidth for all lines, as a first approximation. According to such a model, the absorption coefficient spectrum would be the superposition of a continuous background and broad lines of water vapor. The spectral resolution of our spectrometry measurement can exhibit such an absorption coefficient spectrum. But the inversion method does not compute such a spectrum (Fig. 16). We obtain a continuous spectrum without the right spectral lines. However, the contribution of water vapor is conceivable because of the effects of the pressure. The thermodynamic states attained in the NM reaction products (local constant volume explosions of shocked NM at 2810 K and 14–17 GPa, superdetonation at 3166 K and 25.1–31.6 GPa, detonation at 3253 K and 11.4–13.2 GPa, according to the measurements and the thermochemical calculations) are unusual and out of the validity range of the known data of gas and particle emission spectra. In such conditions of temperature and pressure, the main cause of lines broadening can be the pressure effect (Doppler lines broadening from high temperature is negligible). But other effects are conceivable. The convolution of the molecules collisions effect and autoabsorption is a possible explanation of continuous spectral absorption coefficient. The number of molecules per unit volume is high: the molecular density is about 10^{29} molecules/m^3 at 3500 K and 15 GPa. In such a thermodynamic state, the mean distance between molecules ($\sim 10^{-10}$ m) is close to their mean diameter collision, so that no model exists at present. In dense plasma, highly nonhomogeneous and optically thick (as the detonation products), autoabsorption of lines can lead to an excessive broadening and a total reversal of the lines. The idea of nonthermal emissivity emerges in the work of Gruzdkov and Gupta about shock-induced decomposition of NM [34]. They measured the emission spectrum between 0.4 and 0.75 µm of NM shocked at 16.7 GPa under a stepwise loading process and a peak appeared at 0.65 µm. They explained it as luminescence from reaction products, possibly NO_2. The fluorescence of NO_2 can indeed last 44 µs [35] so our emission measurements during the SDT could record the chemiluminescence of NO_2 after its formation during the NM decomposition. However, as already said, comparison of the radiance spectra during the steady-state detonation and after the interaction with the LiF window shows the same shape (Fig. 10). Indeed the decomposition of NM is finished and the chemiluminescence of NO_2 cannot occur. Moreover, the hot spot temperature is slightly lower than the calculated constant volume adiabatic explosion temperature of shocked NM (Table 3). This temperature is thus compatible with a purely thermal emission, unlike the conclusions of Gruzdkov and Gupta [34]. Therefore, although the absorption coefficient profiles measured and retrieved can hardly be explained in view of today's knowledge at high pressure and temperature, the temperature profiles obtained with the inversion method are compatible with a purely thermal emission mechanism (retrieved temperature values are not slightly different from the temperature calculated with CHEETAH, shown in Table 3).

6. Conclusions

We developed a time-resolved emission spectroscopy device in the visible range 0.3–0.85 µm. Sixteen radiance profiles have been obtained for each experiment of plane shock impact on liquid explosive target at about 8.6 GPa. The combination of other metrological tools and the spectrometer makes it possible to display the different stages of the SDT as described by Chaiken. The calculation of the radiance temperature gives the minimum temperature reached during each stage. For shocked NM, this value reaches 2500 K and during the superdetonation and detonation propagations, respectively 3200 and 3600 K.

The spectral analysis of the emitted intensity related to the temporal analysis shows a particularity in the emission spectrum that appears from the formation of the superdetonation wave. This result could not be recorded by the former pyrometer measurements. The following conclusions on the optical properties during the different steps of the initiation as

well as the propagation of the detonation have been proposed:

- Our results correlated to multiple shock experiments conducted at the CEG [25,26] show that NM remains transparent under shock and confirm that the 2500 K high value of shock temperature are consecutive to local chemical reactions.
- The chemical composition of reaction products changes with the formation of the detonation wave. They are still semitransparent but become optically thick in the range 0.4–0.85 μm. The emission comes from a small-thickness layer just behind the detonation front. Therefore, the common black or gray body assumption cannot be used.
- Reaction products appearing with the superdetonation wave are semitransparent. It seems that they are transparent in the range 0.4–0.6 μm but they absorb light in the range 0.6–0.85 μm, where they are called optically thick.

We carried out a mathematical inversion of the equation of radiative transfer in order to determine the temperature profiles and the absorption coefficient from the radiance measurements. The inversion method is of great interest to obtain temperature profiles during the SDT. With this approach, 80% of the measured spectra can be retrieved. We discussed the measured emission spectrum and the computed absorption coefficient obtained through classical emission models of solid particle and gases. It appears that without precise data at high pressure and high temperature, it is difficult to predict the effect of pressure on emission spectrum. Nevertheless, the inversion method based on thermal emissivity enables to help interpreting the measurements and progressing in the modeling of the SDT.

Acknowledgments

The work described here was carried out with financial support from DGA/SPNuc, for the interest of CEA. Each impact experience was performed at Physics of Explosive Laboratory at CEG with the assistance of ARES and Metrology staff. We are thankful to Regis Serradeill for his advice.

References

[1] B. Léal-Crouzet, Application de la pyrométrie optique à la mesure de température des produits de réaction d'explosifs condensés en régime d'amorçage et de détonation, Ph.D. report, Université de Poitiers, France, 1998.
[2] Y. Kato, Contribution à l'étude des détonations des mélanges hétérogènes de nitrométhane et d'aluminium, Ph.D. report, Université de Poitiers, France, 1978.
[3] P. Hervé, Techniques de l'ingénieur, R2737, 1989.
[4] J.F. Sacadura, Colloque SFT, Nantes, 1990.
[5] L.S. Rothman, C.P. Rinsland, A. Goldman, et al., J. Quantum Spectrosc. Radiat. Transfer 60 (5) (1996) 665–710.
[6] N. Jacquinet-Husson, E. Arié, J. Ballard, et al., J. Quantum Spectrosc. Radiat. Transfer 62 (1999) 205–254.
[7] P. Chelin, V. Pina, P. Hervé, J. Phys. IV France 10 (2000) 197–204.
[8] W.G. Von Holle, C. Tarver, in: 7th Symposium (International) on Detonation, 1981, p. 818.
[9] H. Xianchu, H. Changbung, K. Shufong, in: 8th Symposium (International) on Detonation, Albuquerque, NM, 1985, p. 567.
[10] J.L. Gardner, T.P. Jones, M.R. Davies, High Temperatures High Pressures 10 (1981) 459–466.
[11] C. Le Gallic, C. Mabire, P. Bouinot, G. Baudin, in: 51st ARA Meeting, Madrid, 2000.
[12] B. Léal-Crouzet, G. Baudin, J.C. Goutelle, H.N. Presles, in: 11th Symposium (International) on Detonation, Snowmass, 1998, p. 353.
[13] P.B. Coates, High Temperatures High Pressures 20 (1988) 433–441.
[14] V. Bouyer, in: 52nd ARA Meeting, Québec, 2001.
[15] B. Léal-Crouzet, G. Baudin, H.N. Presles, Combust. Flame 122 (1998) 463–473.
[16] R.F. Chaiken, J. Chem. Phys. 33 (1960) 760–768.
[17] V. Bouyer, Etude de la transition choc-détonation du nitrométhane par spectrométrie d'émission, Ph.D. report, Université Paris X, France, 2002.
[18] P.A. Urtiew, Acta Astronautica 3 (1976) 555–566.
[19] M. Sellam, H.N. Presles, C. Brochet, in: 8th Symposium (International) on Detonation, Albuquerque, 1985, p. 425.
[20] A.N. Dremin, S.D. Savrov, Zh. Prikl. Mekh. Techn. Fis. 1 (1965) 103–105.
[21] V. Bouyer, G. Baudin, C. Le Gallic, P. Hervé, in: M.D. Furnish, N.N. Thadhani, Y. Horie (Eds.), Shock Compression of Condensed Matter—2001, in: AIP Conference Proceedings, 2002.
[22] C.S. Yoo, N.C. Holmes, P.C. Souers, in: Symposium on Decomposition, Combustion and Detonation Chemistry of Energetic Materials, Boston, 1995, vol. 418, pp. 397–406.
[23] P.C. Lysne, D.R. Hardesty, J. Chem. Phys. 39 (12) (1973) 6512–6523.
[24] J.M. Winey, G.E. Duvall, M.D. Knudson, Y.M. Gupta, J. Chem. Phys. 113 (17) (2000) 7492–7501.
[25] G. Baudin, C. Le Gallic, R. Serradeill, in: Symposium HDP V, Hautes pressions dynamiques, Saint-Malo, France, 2003, p. 241.
[26] R. Serradeill, C. Le Gallic, P. Bouinot, G. Baudin, in: Symposium HDP V, Hautes pressions dynamiques, Saint-Malo, France, 2003, p. 155.
[27] L.E. Fried, W.M. Howard, P.C. Souers, CHEETAH 2.0 User's Manual, Rev. 5, Lawrence Livermore National Lab., 1998.
[28] D. Baillis, J.F. Sacadura, J. Quantum Spectrosc. Radiat. Transfer 67 (2000) 327–363.

[29] N.W. Winter, F.H. Ree, in: 11th Symposium (International) on Detonation, 1998, pp. 480–489.
[30] V. Bouyer, G. Baudin, C. Le Gallic, I. Darbord, P. Hervé, in: 12th Symposium (International) on Detonation, San Diego, 2002.
[31] F. Clément, G. Chavent, Détermination des profils de température pendant la détonation d'un explosif liquide, le nitrométhane [Determination of Temperature Profiles during the Detonation of a Liquid Explosive: Nitromethane], Report 4641, INRIA Rocquencourt, France, 2002; available at http://www.inria.fr/rrrt/rr-4641.html.
[32] M.F. Modest, Radiative Heat Transfer, McGraw–Hill, 1993, Chaps. 3, 9, 10.
[33] C.L. Tien, B.L. Drolen, in: T.C. Chawla (Ed.), Annual Review of Numerical Fluid Mechanics and Heat Transfer, vol. 1, Hemisphere, 1987, p. 1.
[34] Y.A. Gruzdkov, Y.M. Gupta, J. Phys. Chem. A 102 (1998) 2322–2331.
[35] G. Herzberg, Molecular Spectra and Molecular Structure, vol. 3. Electronic Spectra and Electronic Structure of Polyatomic Molecules, Masson, Paris, 1992.
[36] F.G. Smith (Ed.), Atmospheric Propagation of Radiation, SPIE Optical Engineering Press, 1993, p. 43.